ANTIOXIDANTS & REDOX SIGNALING
Volume 32, Number 18, 2020

DOI: 10.1089/ars.2019.7730

Discoveries

FORUM ORIGINAL RESEARCH COMMUNICATION

Nuclear Factor Erythroid-Derived 2-Like 2-Induced Reductive Stress Favors Self-Renewal of Breast Cancer Stem-Like Cells *via* the FoxO3a-Bmi-1 Axis

Do-Hee Kim,[1,2] Jeong-Hoon Jang,[1] Ok-Seon Kwon,[3] Hyuk-Jin Cha,[1,3] Hyo-Jin Youn,[1] Kyung-Soo Chun,[4] and Young-Joon Surh[1–3,5]

Abstract

Aims: A subpopulation of cancer cells, termed cancer stem cells (CSCs), has stemness properties, such as self-renewal and differentiation, which drive cancer recurrence and tumor resistance. CSCs possess enhanced protection capabilities to maintain reduced intracellular levels of reactive oxygen species (ROS) compared with nonstem-like cancer cells. This study investigated whether reductive stress could regulate self-renewal activity in breast CSCs.
Results: We found that manifestation of stemness in breast cancer stem-like cells was associated with an elevated production of reduced glutathione (GSH) maintained by upregulation of glutamate cysteine ligase catalytic subunit (GCLC) and consequently, lowered ROS levels. This was accompanied by upregulation of phospho-AMP-activated protein kinase, FoxO3a, and Bmi-1. Notably, expression of nuclear factor erythroid-derived 2-like 2 (Nrf2) protein was substantially increased in cells undergoing sphere formation. We noticed that expression of Bmi-1 was inhibited after introduction of Nrf2 short interfering RNA into MCF-7 mammosphere cells. Silencing of Nrf2 expression suppressed the xenograft growth of subcutaneously or orthotopically injected human breast cancer cells.
Innovation: Association between Nrf2 and self-renewal signaling in CSCs has been reported, but the underlying molecular mechanism remains largely unresolved. This study demonstrates the Nrf2-mediated signaling pathway in maintenance of reductive stress in breast CSCs.
Conclusion: Nrf2 overactivation in breast CSCs upregulates GCLC expression and consequently enhances GSH biosynthesis with concurrent reduction in intracellular ROS accumulation, thereby provoking the reductive stress. The consequent upregulation of nuclear FoxO3a and its binding to the promoter of the gene encoding Bmi-1 account for the self-renewal activity of breast cancer stem-like cells and their growth in a xenograft mouse model. *Antioxid. Redox Signal*. 32, 1313–1329.

Keywords: breast cancer stem cells, self-renewal, redox regulation, reductive stress, Nrf2, FoxO3a

Introduction

CANCER STEM CELLS (CSCs) are defined as a small subset of cells within the tumor microenvironment, which have the intrinsic capability of self-renewal and differentiation (8). The discovery of CSCs and elucidation of their role in cancer recurrence have helped better understand tumor development, metastasis, and resistance to chemo-/radiotherapy. Some signaling molecules involved in the maintenance of CSCs include Hedgehog, Notch, and Bmi-1 (6). Among these, overexpression of Bmi-1 contributes to the manifestation of the phenotype and self-renewal activity of CSCs in

[1]Tumor Microenvironment Global Core Research Center, Seoul National University, Seoul, South Korea.
[2]Department of Molecular Medicine and Biopharmaceutical Sciences, Graduate School of Convergence Science and Technology, Seoul National University, Seoul, South Korea.
[3]Department of Pharmacy, College of Pharmacy, Seoul National University, Seoul, South Korea.
[4]Department of Pharmacy, College of Pharmacy, Keimyung University, Daegu, South Korea.
[5]Cancer Research Institute, Seoul National University, Seoul, South Korea.

Innovation

Cancer stem cells (CSCs) possess enhanced protection capabilities against oxidative stress induced by reactive oxygen species (ROS) compared with nonstem-like cancer cells. In this study, we investigated whether reductive stress could regulate self-renewal activity in breast CSCs. The manifestation of stemness in CSC-like breast cancer cells was associated with an elevated ratio of reduced/oxidized glutathione and consequently, lowered ROS levels. Therefore, activation of nuclear factor erythroid-derived 2-like 2-mediated FoxO3a-Bmi1 signaling accounts for self-renewal activity, and regulation of redox status may provide therapeutic strategies in breast CSCs.

some solid tumors (23, 35). It also promotes epithelial–mesenchymal transition and enhances tumorigenicity (31). In pancreatic cancer cells, increased levels of Bmi-1 have been found in tumor-initiating cell populations characterized by the $CD44^+/CD24^+/ESA^+$ marker, which contributes to CSC-like invasive features (35).

It is noteworthy that CSCs maintain relatively low levels of reactive oxygen species (ROS) (32). Diehn *et al.* have reported that lower ROS levels in mammary CSCs might confer their resistance to ionizing radiation (9). It is hence speculated that low ROS content in CSCs is accompanied by disturbances in cell cycle regulation, which may account for their dormancy (42). Chen *et al.* found that treatment of hematopoietic stem cells with the antioxidant *N*-acetylcysteine resulted in the acquisition of stemness characteristics (5).

In general, expression of cellular antioxidant defense proteins is mainly regulated by the redox-sensitive transcription factor, nuclear factor erythroid-derived 2-like 2 (Nrf2) (29). Reduced glutathione (GSH) is a principal antioxidant molecule responsible for the elimination of ROS. GSH production is catalyzed by the glutamate cysteine ligase complex modifier subunit and glutamate cysteine ligase catalytic subunit (GCLC), under the control of Nrf2 (44). Recently, association between Nrf2 and self-renewal signaling in CSCs has been reported (38, 46, 49), but the underlying molecular mechanism remains largely unresolved.

Forkhead box O (FoxO) family transcription factors function as cellular redox sensors. Their transcriptional activities are affected by the alteration of intracellular and extracellular redox status (21). FoxOs play a critical role in enhancing self-renewal capability of stem cells (45). Bmi-1 is a key molecule involved in the maintenance of stem cells as well as cancer development (41). Here, we report that breast CSCs maintain low levels of intracellular ROS by upregulating Nrf2-induced expression of GCLC, thereby maintaining self-renewal activity *via* the FoxO3a-Bmi1 axis.

Results

The intracellular redox status is critical for the manifestation of stemness in breast cancer stem-like cells

It has been reported that CSCs, in general, exhibit lower ROS levels than nonstem cells (9, 39), which is maintained by upregulation of antioxidant gene expression. The correlation between recurrent breast cancer and antioxidant gene expression was assessed by gene set enrichment analysis (GSEA) of clinical data deposited from GSE2034. Through the GSEA analysis, we found that the ROS-related gene set was significantly enriched in breast tumor from nonrelapsed patients, whereas biosynthetic and metabolic processes of ROS were downregulated in the relapsed breast cancer (Fig. 1A). When MCF-7 cells were grown as mammospheres for 5 days, the cellular ROS level was found to be decreased compared with that in parent cells as measured by fluorescence-activated cell sorting (FACS) analysis (Fig. 1B and Supplementary Fig. S1A).

We isolated $CD24^{low}/CD44^{high}$ breast cancer stem-like cells from MCF-7 mammospheres by use of the FACSAria™ cell sorter, and the intracellular accumulation of ROS was measured by 2′,7′-dichlorofluorescein diacetate (DCF-DA) staining. We observed that $CD24^{low}/CD44^{high}$ breast cancer stem-like cells contain low levels of ROS when compared with parent MCF-7

FIG. 1. Intracellular ROS levels, GSH contents, and expression of GCLC are crucial for the self-renewal ability of breast cancer stem-like cells. (A) GSEA demonstrated the regulation of the ROS-related signaling in breast cancer tissues with or without relapse. **(B)** MCF-7 cells were grown as mammospheres for 5 days, and then intracellular ROS levels were determined by FACS analysis of cells after DCF-DA staining. **(C)** The mammosphere cells were analyzed by FACS for sorting the $CD24^{low}/CD44^{high}$ breast cancer stem-like cells. The intracellular ROS levels were then compared by DCF-DA staining in parent MCF-7 cells and MCF-7-derived $CD24^{low}/CD44^{high}$ cells. **(D)** Parent MCF-7 cells and mammospheres were incubated with DHE or MitoSOX for 30 min, washed thoroughly, and immediately analyzed by FACS. **(E)** After sorting mammosphere cells using respective CD24 and CD44 antibodies, intracellular GSH levels and the GSH/GSSG ratio were measured by using the GSH-Glo™ Glutathione Assay Kit. **(F)** The expression of CD44, GCLC, and Bmi-1 proteins was analyzed by immunoblot analysis using total cell lysates with different CD24 and CD44 phenotypes sorted from mammospheres. **(G, H)** MCF-7 mammosphere cells were treated with BSO or H_2O_2 at indicated concentrations. Total protein extracts from mammosphere cells were subjected to Western blot analysis using anti-Bmi-1 antibody. Actin was measured as an indicator of equal amounts of protein loaded. **(I–K)** MCF-7 cells were cultured on ultralow adherence plates for 5 days to generate primary mammospheres. The primary mammospheres were dissociated and cultured for additional 5 days to generate secondary mammospheres. MCF-7 secondary mammosphere cells were treated with 0.1 m*M* BSO or 2 m*M* GSH-MEE for 3 days, and then the self-renewal capacity of MCF-7 cells was measured in terms of sphere formation. Pictures are representative phase-contrast photomicrographs of mammospheres, and graph bars are presented as the number of sphere cells ($n = 3$ per each treatment group, size >100 μm). Scale bar, 100 μm. BSO, buthionine sulfoximine; DCF-DA, 2′,7′-dichlorofluorescein diacetate; DHE, dihydroethidium; FACS, fluorescence-activated cell sorting; GCLC, glutamate cysteine ligase catalytic subunit; GSEA, gene set enrichment analysis; GSH, reduced glutathione; GSH-MEE, glutathione-reduced ethyl ester; GSSG, oxidized glutathione; H_2O_2, hydrogen peroxide; NES, normalized enrichment score; Nrf2, nuclear factor erythroid-derived 2-like 2; ROS, reactive oxygen species. Color images are available online.

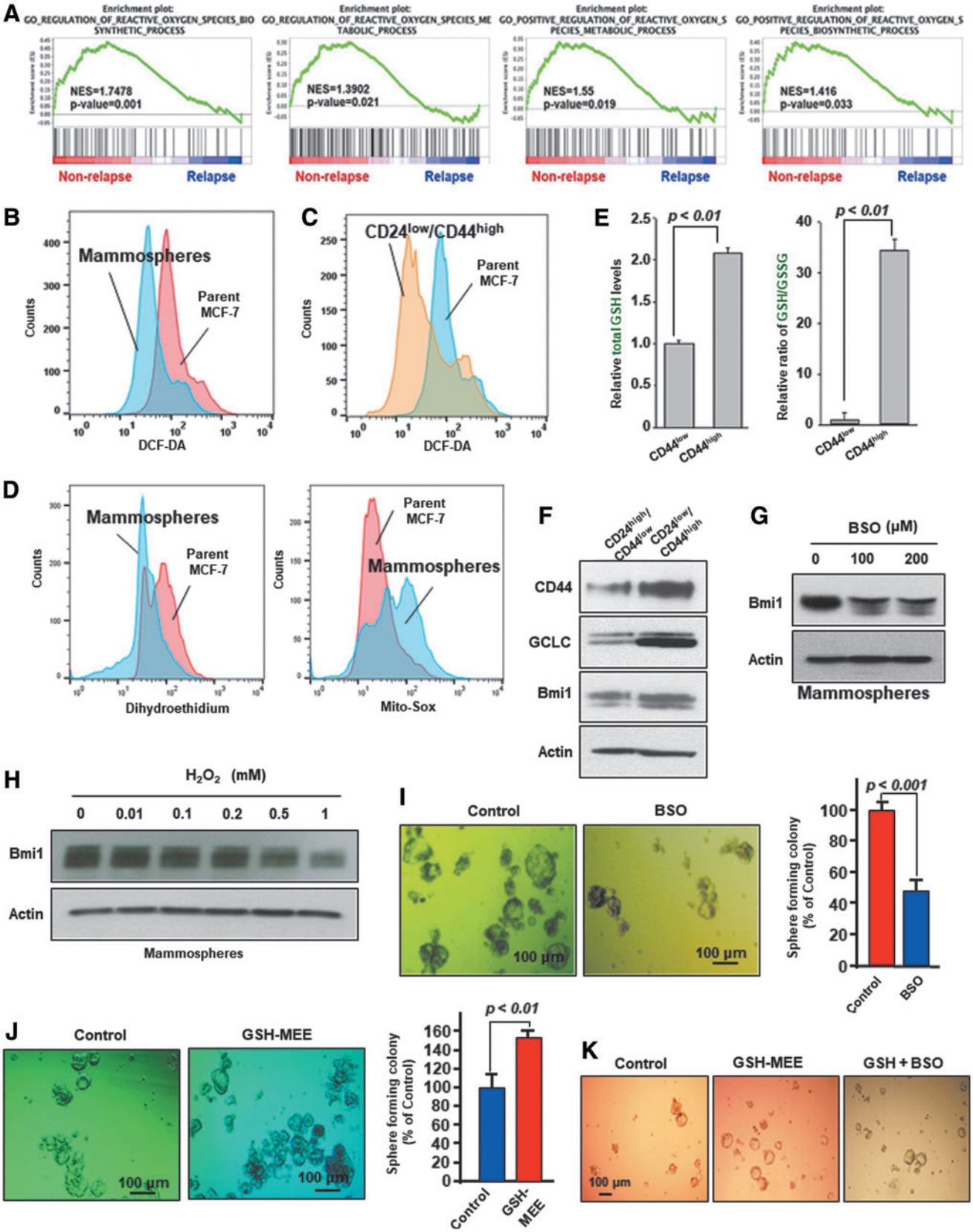

cells (Fig. 1C and Supplementary Fig. S1B). In general, superoxides in the cytoplasm and mitochondria are detected by using dihydroethidium (DHE) and MitoSox dye, respectively (33). We observed that mammospheres derived from MCF-7 cells exhibited a decreased ROS level detected by DHE staining, whereas MitoSox staining did not show any significant changes (Fig. 1D).

GSH is the most important hydrophilic antioxidant that protects cells from exogenous and endogenous toxicants, including ROS (4). The ratio of GSH to an oxidized form (GSSG) has been considered as an indicator of cellular redox status. Thus, the reduced ratio of GSH/GSSG is an indication of oxidative stress, whereas an increased ratio is indicative of reductive stress (4). We noted that $CD24^{low}/CD44^{high}$ breast cancer stem-like cells exhibit the higher GSH/GSSG ratio as well as total intracellular GSH than $CD24^{high}/CD44^{low}$ cells sorted from MCF-7 mammospheres (Fig. 1E). In addition, there was a concurrent increase of CD44, GCLC, and Bmi-1 protein expression in $CD24^{low}/CD44^{high}$ breast cancer stem-like cells (Fig. 1F and Supplementary Fig. S1C).

To further verify that the redox status in mammosphere formation is essential for regulation of Bmi-1-mediated self-renewal signaling, we performed the immunoblot analysis using anti-Bmi1 antibody after the treatment of MCF-7 mammospheres with buthionine sulfoximine (BSO), an inhibitor of GCLC, and also with hydrogen peroxide (H_2O_2). As shown in Figure 1G and H, treatment of mammosphere cells with these compounds provoking prooxidant status resulted in the decreased Bmi-1 protein expression (Supplementary Fig. S1D, E), suggesting that the ROS production might render these cells incompetent for self-renewal activity. Thus, we intended to determine whether GCLC could regulate the self-renewal activity in the process of generating the third-generation mammospheres. Depletion of GSH by BSO treatment led to a diminution of the number and the size of mammospheres (Fig. 1I). In contrast, treatment of MCF-7 mammospheres with glutathione-reduced ethyl ester (GSH-MEE), a membrane permeable derivative of GSH, resulted in the increased size and the number of mammospheres (Fig. 1J). Notably, the GSH-mediated increase in mammospheres was abrogated by BSO treatment (Fig. 1K).

Furthermore, we examined the GCLC mRNA expression levels in different CD24/CD44 phenotypes using a published database (GSE2034). As shown in Supplementary Figure 2A, the $CD24^{low}/CD44^{high}$ group expressed higher amount of GCLC than did the $CD24^{high}/CD44^{low}$ group in breast cancer patients. Further, GCLC expression correlated with poor clinical outcome. In the GCLC-amplified group, the probability of relapse-free survival was significantly higher than that in the low GCLC expression group (Supplementary Fig. S2B). To determine whether CD44 could be regulating the expression of GCLC transcripts in the patient tumor, we evaluated trends in transcript abundance of each gene in the breast cancer patients with relapse. Particularly, the correlation between CD44 and GCLC significantly increased in relapse patient samples of GSE1456 (Supplementary Fig. S2C).

GCLC-mediated GSH production upregulates expression of FoxO3a and Bmi-1 in mammosphere cells

Recently, Hu *et al.* have reported that heterogeneity of CSCs expressing different CD44 isoforms in breast cancer is associated with a CSC subpopulation with enhanced lung metastasis capacity (15). In line with this notion, there is an increase in the expression of CD44s and CD44v types, GCLC and Bmi-1 in third-generation mammospheres as compared with parent cells (Fig. 2A and Supplementary Fig. S3A). Sox-2 was used as a sphere cell marker. To determine the possible involvement of GCLC in regulating the expression of CD44 and Bmi-1 transcripts in patient tumor samples, we evaluated trends in transcript abundance of each gene in the breast cancer samples of GSE1456. As shown in Figure 2B, GCLC expression was well correlated with the levels of CD44 and Bmi-1 gene expression.

It has been demonstrated that overexpression of anti-apoptotic proteins, such as Bcl-2, causes redistribution of GSH to the nucleus, thereby altering the nuclear redox status (24). Notably, nuclear GSH plays a role in regulating cellular proliferation, and influences both telomerase activity and histone function (12). To investigate the subcellular distribution of GSH in breast cancer stem-like cells, mammospheres were incubated with the 5-chloromethylfluorescein diacetate fluorescent probe for 30 min. Next, the images were taken by light microscopy to capture red fluorescence of nuclei and green fluorescence for GSH. As illustrated in Figure 2C, GSH was detected in the nucleus as well as cytoplasm of mammosphere cells.

It has been reported that FoxO activity is regulated by intracellular GSH and ROS (13, 21). To determine whether intracellular GSH can induce expression of FoxO3a, thereby regulating Bmi-1, MCF-7 cells were treated with GSH-MEE for 48 h. As shown in Figure 2D, exogenous supply of GSH resulted in upregulation of FoxO3a and Bmi-1 (Supplementary Fig. S3B). In contrast, expression of Bmi-1 and FoxO3a was decreased in BSO-treated MCF-7 mammosphere cells (Fig. 2E and Supplementary Fig. S3C). Moreover, mammosphere formation was accompanied by FoxO3a phosphorylation at the Ser 7 residue, and subsequently nuclear accumulation in MCF-7 cells (Fig. 2F, G and Supplementary Fig. S3D).

GSH induces phosphorylation of AMP-activated protein kinase and FoxO3a for self-renewal activity of breast cancer stem-like cells

It has been reported that the crosstalk between AMP-activated protein kinase (AMPK) and FoxO under metabolic stress is essential for redox maintenance (48). We found that there was a robust increase in phospho-AMPK (Thr172) and P-FoxO3a (Ser7) in mammospheres compared with those in parent MCF-7 cells (Fig. 3A, B and Supplementary Fig. S4A). Ho *et al.* have reported that the Ser7 residue of FoxO3a is the only phosphorylation site associated with its nuclear enrichment (14). We found that levels of Bmi-1 protein expression and FoxO3a phosphorylation were decreased in AMPK-knockdown MCF-7 mammosphere cells (Fig. 3C and Supplementary Fig. S4B). Further, phosphorylation of AMPK and FoxO3a was markedly enhanced in MCF-7 mammosphere cells treated with GSH-MEE (Fig. 3D and Supplementary Fig. S4C). Conversely, treatment of GSH-enriched mammospheres with the prooxidant H_2O_2 abrogated the AMPK activation (Fig. 3E and Supplementary Fig. S5A). Moreover, treatment of mammosphere cells with H_2O_2 resulted in decreased expression of both total and phosphorylated FoxO3a proteins (Fig. 3F and Supplementary Fig. S5B). These findings

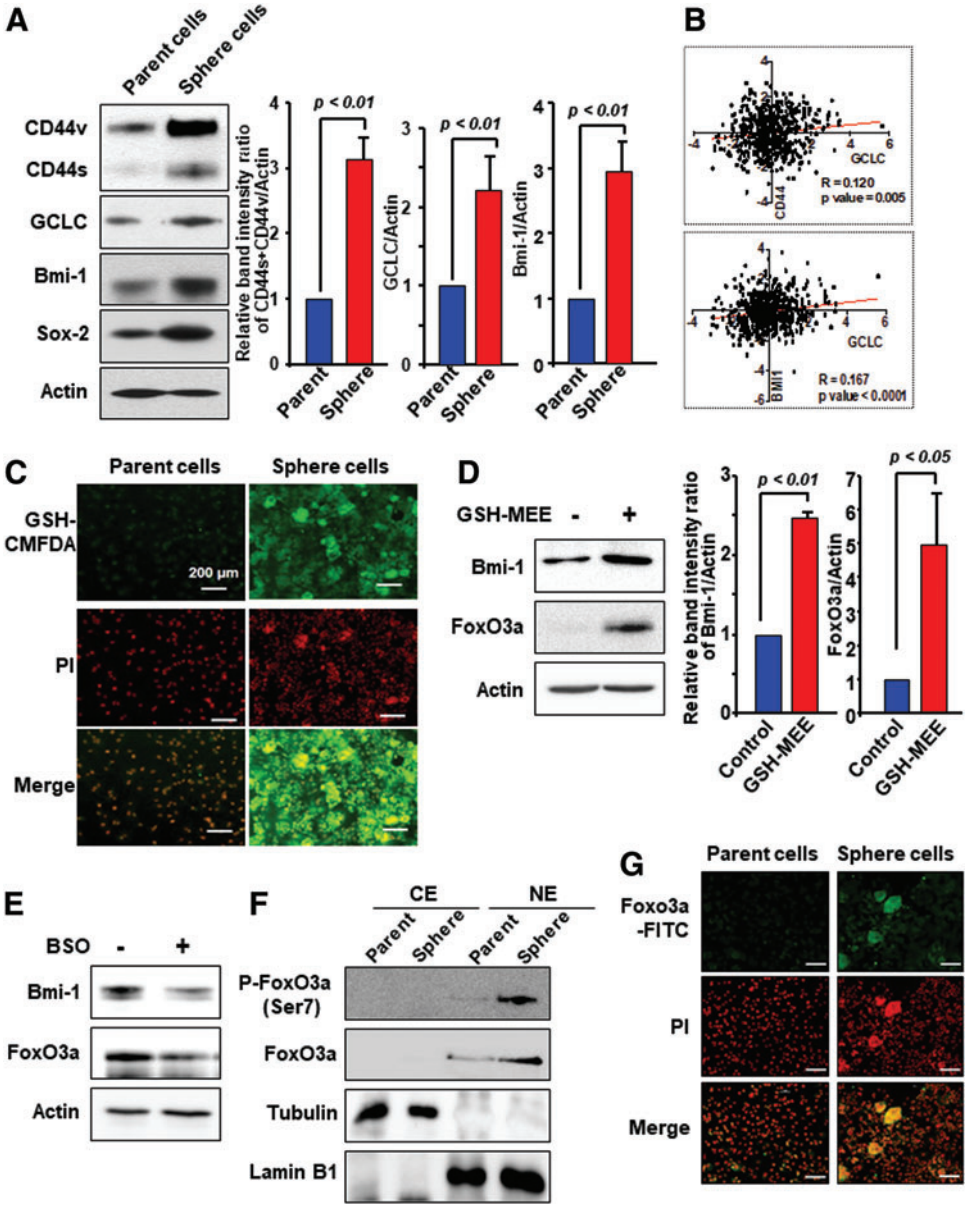

FIG. 2. GCLC-mediated GSH generation induces increased Bmi-1 expression and nuclear distribution of FoxO3a in mammosphere cells. (A) After the generation of mammospheres, expression of CD44, GCLC, and Bmi-1 proteins was determined by immunoblot analysis in MCF-7 parent and sphere-forming cells. Sox-2 was used as a positive control to ensure the mammosphere formation. The levels of total CD44 (CD44s and CD44v), GCLC, and Bmi-1 proteins were normalized to actin, and the corresponding bands were quantified using the Multi Gauge version 3.0 program (Fujifilm). Replicate measurements were typically performed in triplicate. Data are shown as mean values ± SD. **(B)** Indicated gene expression data from breast cancers were analyzed using the cBioportal web interface, and correlation plots with Spearman's correlations are presented. GCLC expression was correlated with the levels of CD44 and Bmi-1 gene expression. **(C)** Parent and mammosphere MCF-7 cells were incubated with the CMFDA probe for 30 min. The images were then taken by light microscopy to capture *red* fluorescence for nuclei and *green* fluorescence for GSH. Scale bar, 200 μm **(D, E)** Primary MCF-7 mammosphere cells were treated with or without 2 m*M* GSH-MEE or 0.1 m*M* BSO for 48 h, and total lysates were prepared and subjected to Western blot analysis using antibodies against Bmi-1 and FoxO3a. Replicate measurements were typically performed in triplicate ($n = 3$). **(F)** Nuclear protein levels of Foxo3a were determined in parent MCF-7 cells and mammospheres by immunoblot analysis. α-Tubulin and Lamin B_1 were used as molecular markers for the cytosolic and nucleus fractions, respectively. **(G)** The nuclear FoxO3a protein level was determined by immunocytochemistry in parent MCF-7 cells and MCF-7-derived sphere-forming cells. Scale bar, 200 μm. CE, cytosolic extract; CMFDA, 5-chloromethylfluorescein diacetate; NE, nuclear extract; PI, propidium iodide. Color images are available online.

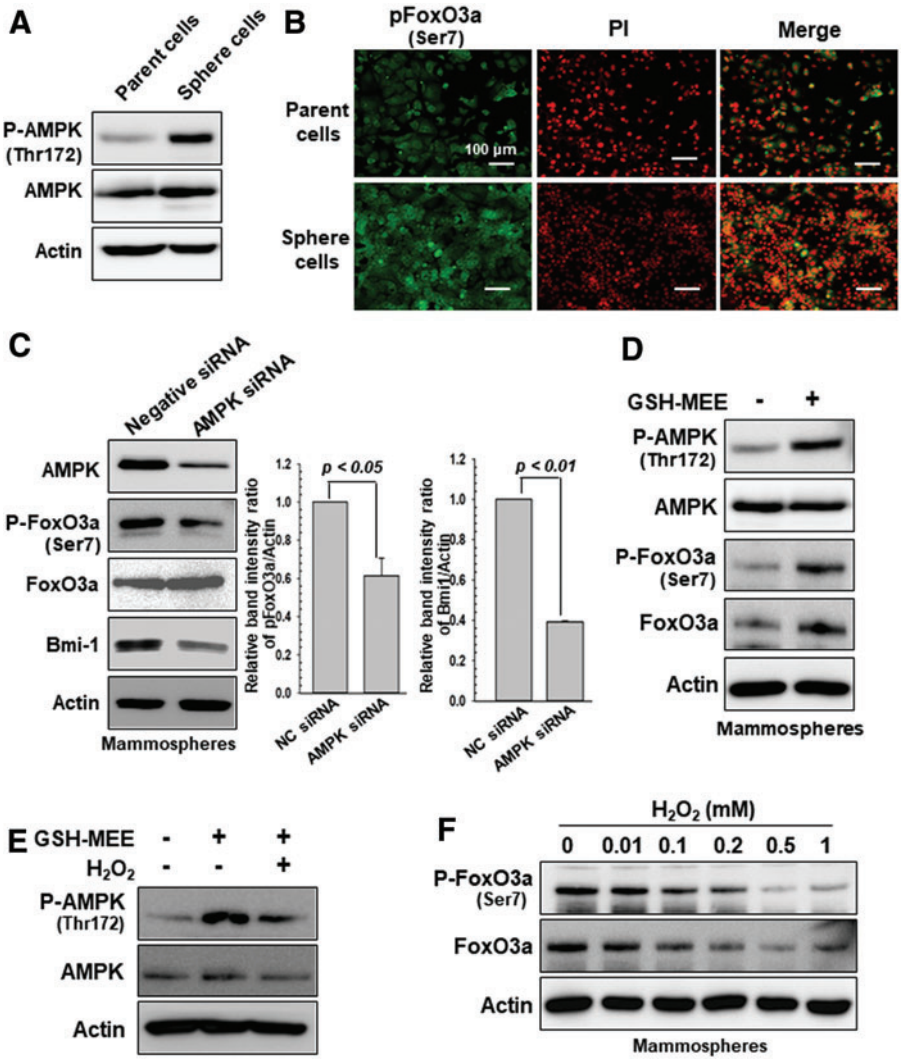

FIG. 3. Phosphorylation of AMPK and FoxO3a by GSH leads to the nuclear localization of FoxO3a. (A) After the generation of mammospheres, expression of P-AMPK (Thr172) and total AMPK was determined by immunoblot analysis in parent MCF-7 and mammosphere cells. **(B)** After the generation of mammospheres, expression of P-FoxO3a (Ser7) was determined by immunocytochemistry in parent MCF-7 and mammosphere cells. Scale bar, 100 μm. **(C)** MCF-7 cells were transfected with scrambled siRNA and AMPK-specific siRNA for 72 h, followed by sphere-forming culture for additional 5 days. Levels of P-FoxO3a and Bmi-1 were determined by Western blot analysis. Relative band intensity of indicated proteins was normalized to actin, and the corresponding bands were quantified using the Multi Gauge. Replicate measurements were typically performed in triplicate ($n = 3$). **(D)** Primary MCF-7 mammosphere cells were incubated with GSH-MEE (2 m*M*) for 48 h. Whole lysates with or without GSH-MEE treatment were prepared and subjected to Western blot analysis for measurement of P-AMPK (Thr172), P-FoxO3a (Ser7), and their respective total forms. **(E)** To determine the phosphorylation of AMPK, MCF-7 mammosphere cells were incubated with GSH-MEE (2 m*M*) for 12 h and incubated with H_2O_2 (200 μM) for another 24 h. **(F)** MCF-7 mammosphere cells were treated with H_2O_2 at indicated concentrations for 48 h. Mammosphere cells were harvested and subjected to immunoblot analysis. AMPK, AMP-activated protein kinase; NC, negative control; P-AMPK, phospho-AMPK; siRNA, short interfering RNA. Color images are available online.

suggest that a redox shift toward GSH accumulation can trigger phosphorylation of AMPK and FoxO3a, which accounts for self-renewal activity of breast cancer stem-like cells.

FoxO3a induces Bmi-1 transcription by directly binding to its proximal promoter

After revealing the FoxO3a upregulation by GSH, we determined whether FoxO3a could regulate the expression of Bmi-1. We noticed that expression levels of Bmi-1 protein and its mRNA transcript were decreased in FoxO3a knockdown MCF-7 mammosphere cells (Fig. 4A, B and Supplementary Fig. S6A). To understand how the Bmi-1 gene expression is regulated by FoxO3a, we analyzed the Bmi-1 promoter region and identified a single putative FoxO3a binding site in the upstream of the transcription start site. The information on the promoter region (promoter ID: BMI1_2) was obtained from a Eukaryotic promoter database. FoxO3a binding to the Bmi-1 promoter was verified by a chromatin immunoprecipitation (ChIP) assay (Fig. 4C).

In addition, the proportion of the $CD44^{high}/CD24^{low}$ cell population in MCF-7 mammospheres was decreased by

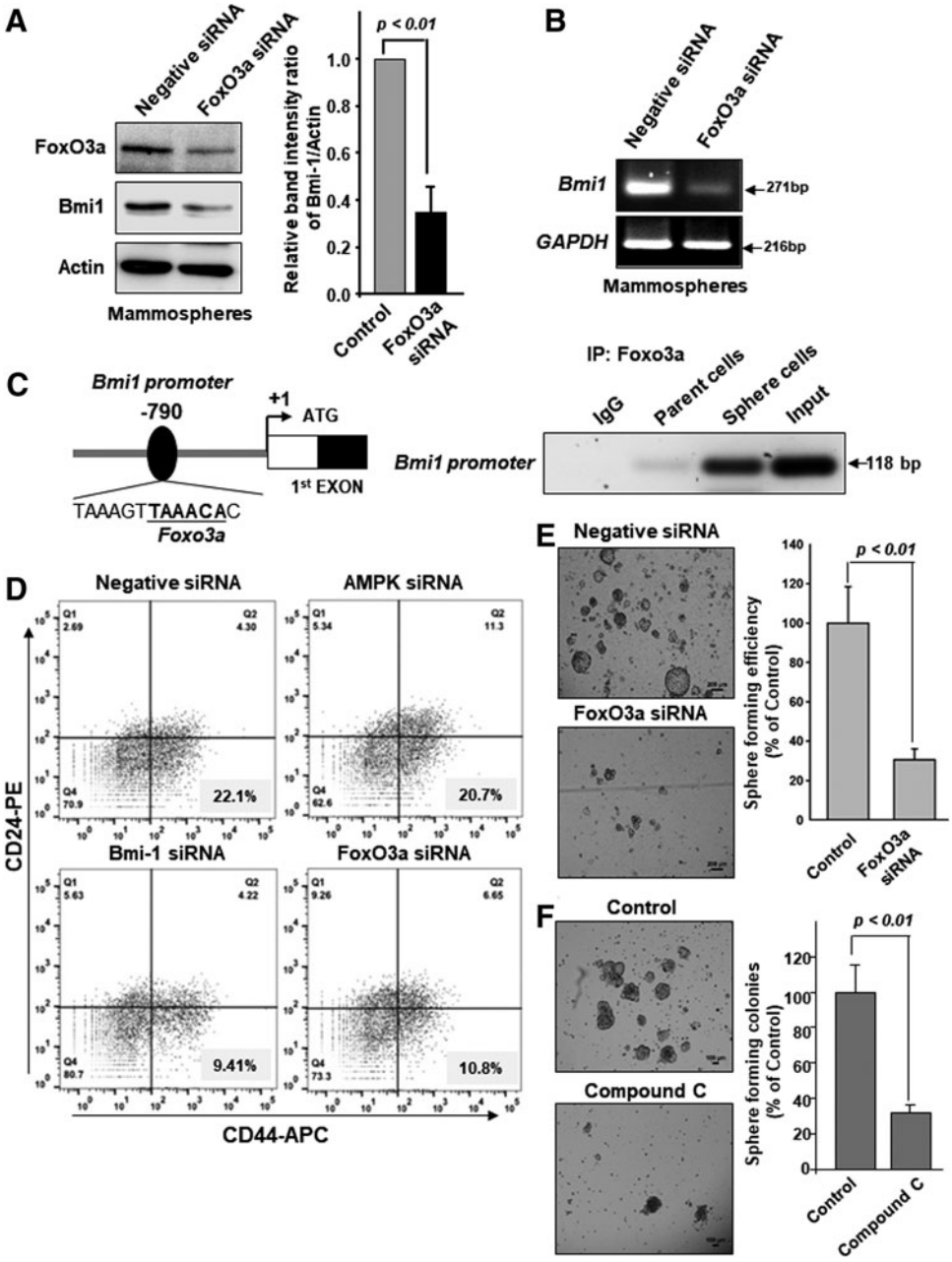

FIG. 4. FoxO3a induces Bmi-1 transcription in MCF-7 mammosphere cells. (A, B) MCF-7 cells were transfected with scrambled siRNA or FoxO3a-specific siRNA for 72 h, followed by sphere-forming culture for additional 5 days. Levels of FoxO3a and Bmi-1 were determined by Western blot **(A)** and/or RT-PCR analyses **(B)**. **(C)** The *left diagram* illustrates the Foxo3a binding site in the Bmi-1 promoter. Protein–DNA complexes from MCF-7 sphere cells were immunoprecipitated with IgG or Foxo3a antibody. Binding of Foxo3a to the promoter region of Bmi-1 gene in MCF-7 mammosphere cells was determined by the ChIP assay. **(D)** MCF-7 cells were transfected with respective specific siRNAs for 72 h, followed by staining sphere-forming cells for additional 5 days with anti-CD44-APC and anti-CD24-PE antibodies. Flow cytometric dot plots represent changes in the proportion of $CD44^{high}/CD24^{low}$ cells. Quadrant analysis of fluorescence intensity of gated cells in FL2 and FL4 channels was from 10,000 events. **(E)** MCF-7 cells were transfected with scrambled siRNA or FoxO3a-specific siRNA for 72 h, followed by sphere-forming culture for additional 5 days. **(F)** MCF-7 cells were cultured on ultralow adherence plates for 5 days to generate primary mammospheres. The primary mammospheres were dissociated and cultured for additional 5 days to generate secondary mammospheres. MCF-7 secondary mammosphere cells were treated with 10 μM compound C for 3 days, and then the self-renewal capacity of MCF-7 cells was measured in terms of sphere formation. Sphere forming colonies were visualized by phase-contrast photomicrograph (magnification $\times 100$) and quantified. Pictures are representative phase-contrast photomicrographs of mammospheres, and graph bars are presented as the mean percentage of sphere cells ($n = 3$ per treatment group, size $>100\,\mu$m). Scale bar, 100 μm. ChIP, chromatin immunoprecipitation; RT-PCR, reverse transcription-polymerase chain reaction.

knockdown of *AMPK*, *Bmi-1,* and *FoxO3a* using target-specific short interfering RNA (siRNA) (Fig. 4D). Use of unstained and singly dye-stained cells as compensation controls is common, so we set the standard for flow cytometry gating (Supplementary Fig. S6B). We also noticed that knockdown of FoxO3a expression in MCF-7 cells abrogated the formation of secondary mammospheres (Fig. 4E). Treatment with compound C, a well-known inhibitor of AMPK, led to a diminution of the number and the size of mammospheres (Fig. 4F). Furthermore, we performed the correlation study with the breast cancer cohort of early breast cancer patients (GSE1456, $n = 159$). The moderate correlation between Foxo3a and Bmi-1 was found (Supplementary Fig. S6C). Taken together, these findings indicate that FoxO3a transcriptionally regulates Bmi-1 to promote self-renewal activity of breast cancer stem-like cells.

Nrf2 activation contributes to self-renewal activity of breast mammosphere cells

Based on the upregulated expression of GCLC, we examined whether the Nrf2 signaling pathway could be activated in breast cancer mammospheres. We observed that expression of Nrf2 protein was substantially increased in cells growing under sphere-forming conditions (Fig. 5A and Supplementary Fig. S7A). In addition, the nuclear accumulation of Nrf2 was evident in the mammospheres derived from MCF-7 cells (Fig. 5B and Supplementary Fig. S7B), which was further verified by immunocytochemical analysis (Fig. 5C). Further, the sphere formation was abrogated by Nrf2 silencing (Fig. 5C). As there was a concomitant increase in the expression of CD44 and Nrf2 in third-generation mammospheres, we explored the involvement of CD44 in self-renewal activity *via* the Nrf2 signaling.

Variant forms of CD44 are likely to be involved in activation of Nrf2-mediated signaling (18). The expression of Nrf2 was markedly inhibited in MCF-7 mammosphere cells silenced for CD44 expression (Fig. 5D and Supplementary Fig. S7C). Notably, the high levels of Nrf2 are significantly related to relapsed breast cancer, according to the GSE2034 dataset (Fig. 5E). Collectively, these findings suggest that activation of Nrf2 responsible for the GCLC upregulation in breast cancer stem-like cells is attributable, at least in part, to CD44. We found the decreased intracellular levels of GSH and increased ROS production in Nrf2-knockdown breast cancer (MDA-MB-231) cells. It is likely that reduced production of GSH may provoke inefficient cellular detoxification of ROS in Nrf2-silenced MDA-MB-231 cells (Fig. 5F, G).

Nrf2 plays a role in the sphere-forming capability of breast cancer cells through upregulation of GCLC and Bmi-1

Next, we examined the expression of Bmi-1 in Nrf2-knockdown or overexpressing breast cancer cells. In general, MDA-MB-231 cells exhibit a higher Nrf2 expression compared with MCF-7 cells (47). As shown in Figure 6A, silencing Nrf2 caused downregulation of the Bmi-1 expression in MDA-MB-231 cells (Supplementary Fig. S8A). Conversely, overexpression of Nrf2 enhanced the mRNA and protein levels of Bmi-1 in MCF-7 cells (Fig. 6B and Supplementary Fig. S8B). We also noticed that knockdown of Nrf2 expression in MCF-7 cells abrogated the formation of secondary mammospheres (Fig. 6C). The proportion of $CD44^{high}/CD24^{low}$ cell population in MCF-7 mammospheres was decreased by knockdown of *Nrf2* using target-specific siRNA, whereas Nrf2 overexpression induced stemness properties (Fig. 6D).

The human GCLC promoter contains the antioxidant response element, which is the *cis*-acting consensus sequence responsible for Nrf2 binding (26). We investigated whether Nrf2 could upregulate GCLC expression in breast cancer stem-like cells, necessary for their self-renewal activity mediated by Bmi-1 expression. For this purpose, two different short hairpin RNAs (shRNAs) targeting Nrf2 were transfected into MDA-MB-231 cells that constitutively express Nrf2. Of these, the sh-Nrf2 (#2) efficiently lowered the levels of Nrf2, GCLC, and Bmi-1 mRNA and protein in MDA-MB-231 cells (Fig. 6E and Supplementary Fig. S8C). Likewise, mammosphere formation was abolished in Nrf2-silenced MDA-MB-231 cells (Fig. 6F). Moreover, expression of GCLC and Bmi-1 as well as phosphorylation of AMPK and FoxO3a was decreased in Nrf2-knockdown MDA-MB-231 cells (Fig. 6G and Supplementary Fig. S9). These results suggest that Nrf2 overactivation upregulates GCLC, and subsequently Bmi-1 responsible for self-renewal capability of breast cancer stem-like cells.

Knockdown of Nrf2 attenuates the tumorigenicity of breast cancer cells and mammospheres in vivo

To assess the oncogenic role of Nrf2 in the mammary cancer progression, athymic nude mice were subcutaneously injected with MDA-MD-231 cells transfected with either the control or Nrf2-specific shRNA. In MDA-MB-231 xenografts, Nrf2-shRNA introduction suppressed the tumor growth (Fig. 7A). Knockdown of Nrf2 significantly reduced the size of tumors derived from MDA-MB-231 cells in the xenograft mouse model (Fig. 7B). We confirmed reduced Nrf2 expression by immunohistochemical (IHC) staining of tumor tissues, and quantification of IHC image was performed by ImageJ analysis (Fig. 7C and Supplementary Fig. S10). It was accompanied by decreased expression of GCLC, FoxO3a, and Bmi-1 proteins (Fig. 7D and Supplementary Fig. S11).

In another experiment, MDA-MB-231 sphere-forming cells transfected with lentivirus encoding Nrf2 shRNA or control shRNA were transplanted orthotopically into the fourth inguinal mammary fat pads of female athymic nude mice. After 10 weeks of injection, the mice were anesthetized using isoflurane and *in vivo* tumor green fluorescence protein (GFP) fluorescence was measured by the *in vivo* imaging system (IVIS) spectrum computed tomography (CT). The mice injected with control shRNA cells were able to form tumors more rapidly than those with Nrf2-knockdown cells (Fig. 7E). Overall morphology of the tumor was visualized with hematoxylin and eosin staining (Supplementary Fig. S12). IHC analysis showed a relatively weak staining of Bmi-1 in tumor tissues of mice transplanted with Nrf2-knockdown sphere-forming cells (Fig. 7F and Supplementary Fig. S13).

Discussion

There has been increasing evidence for a causal relationship between intracellular redox status and manifestation of

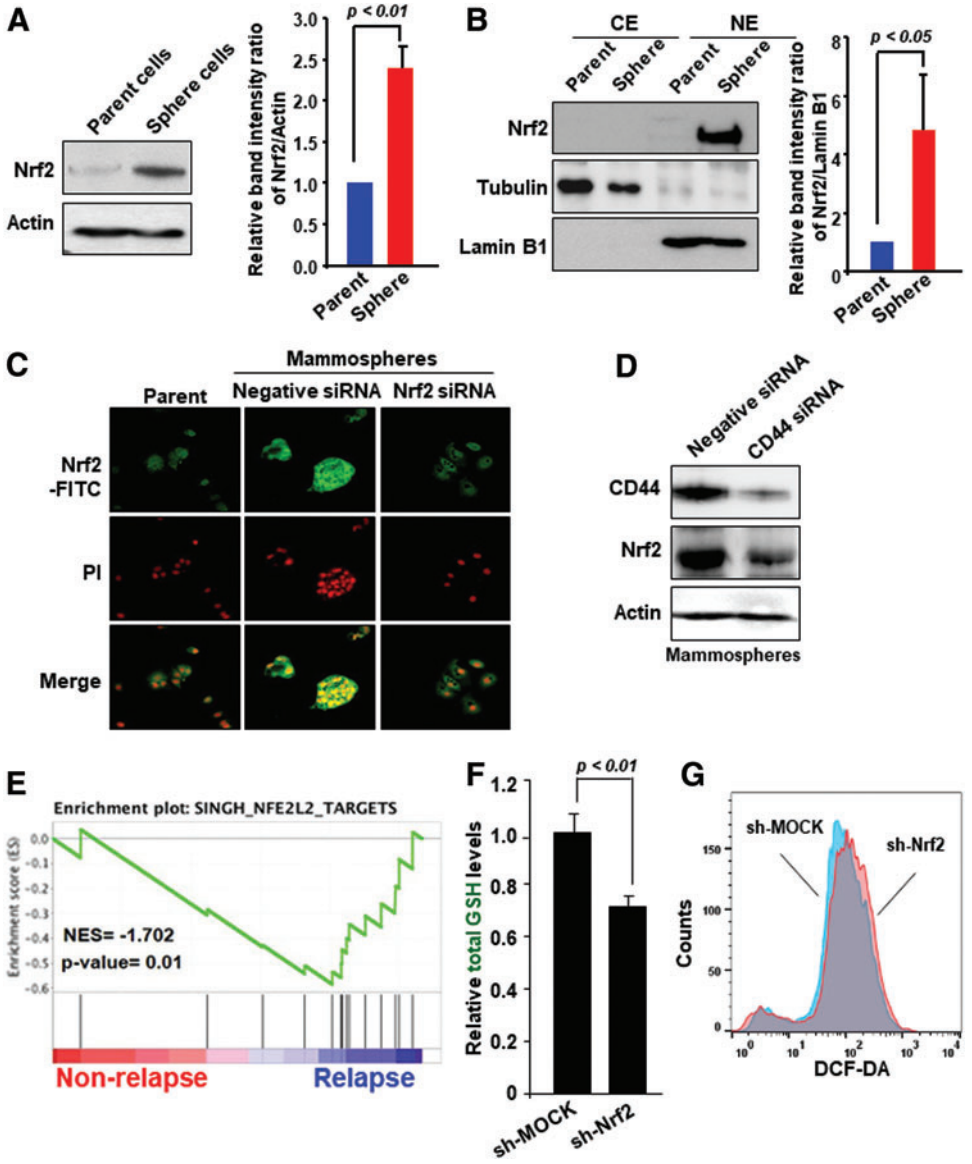

FIG. 5. The possible involvement of Nrf2 activation in breast mammosphere cells. (A) MCF-7 cells were cultured in ultralow adherence plates for generating the third-generation mammospheres, and then expression of Nrf2 protein was assessed by Western blot analysis. Relative band intensity of indicated proteins was normalized to actin, and the corresponding bands were quantified using the Multi Gauge. Replicate measurements are typically performed in triplicate ($n = 3$). **(B, C)** Nuclear Nrf2 protein levels were determined in parent MCF-7 cells and mammospheres by immunoblot analysis **(B)** and immunocytochemistry **(C)**. Tubulin and Lamin B_1 were used as molecular markers for the cytosolic and nucleus fractions, respectively. **(D)** MCF-7 cells were transfected with *CD44* siRNA or negative control siRNA for 48 h, followed by incubation for an additional 5 days to measure mammosphere formation. After sphere formation for 5 days, total cell lysates from mammosphere cells were subjected to Western blot analysis to determine the expression of CD44 and Nrf2. **(E)** GSEA enrichment plot of Nrf2 gene expression in breast cancer tissues with or without relapse. **(F)** Intracellular GSH levels in control and Nrf2-shRNA expressing MDA-MB-231 cells were measured by using the GSH-Glo Glutathione Assay Kit. **(G)** Control and Nrf2-shRNA expressing MDA-MB-231 cells were incubated with DCF-DA, and then the intracellular ROS levels were measured by FACS analysis. shRNA, short hairpin RNA. Color images are available online.

stemness (9, 39). It has been known that CSCs maintain reduced levels of ROS compared with nonstem cells (30, 39). CSCs retaining a low level of ROS exhibit elevated expression of stemness-associated molecules such as Notch-1 and telomerase, which confers a self-renewal potential (16, 32).

Paul *et al.* have identified complex crosstalk between dynamic intracellular ROS flux and Nrf2 in the airway basal stem cells, whereby Nrf2 activates the Notch pathway to stimulate self-renewal activity (32). In addition, several recent studies have revealed the role of Nrf2 in the manifestation and maintenance of CSCs. Thus, the total expression and nuclear translocation of Nrf2 increase under the sphere-forming conditions, which enhance self-renewal activity (37, 38). However, it remains largely unresolved how the accumulation of Nrf2 expression contributes to the self-renewal activity. We also observed that the number and the size of

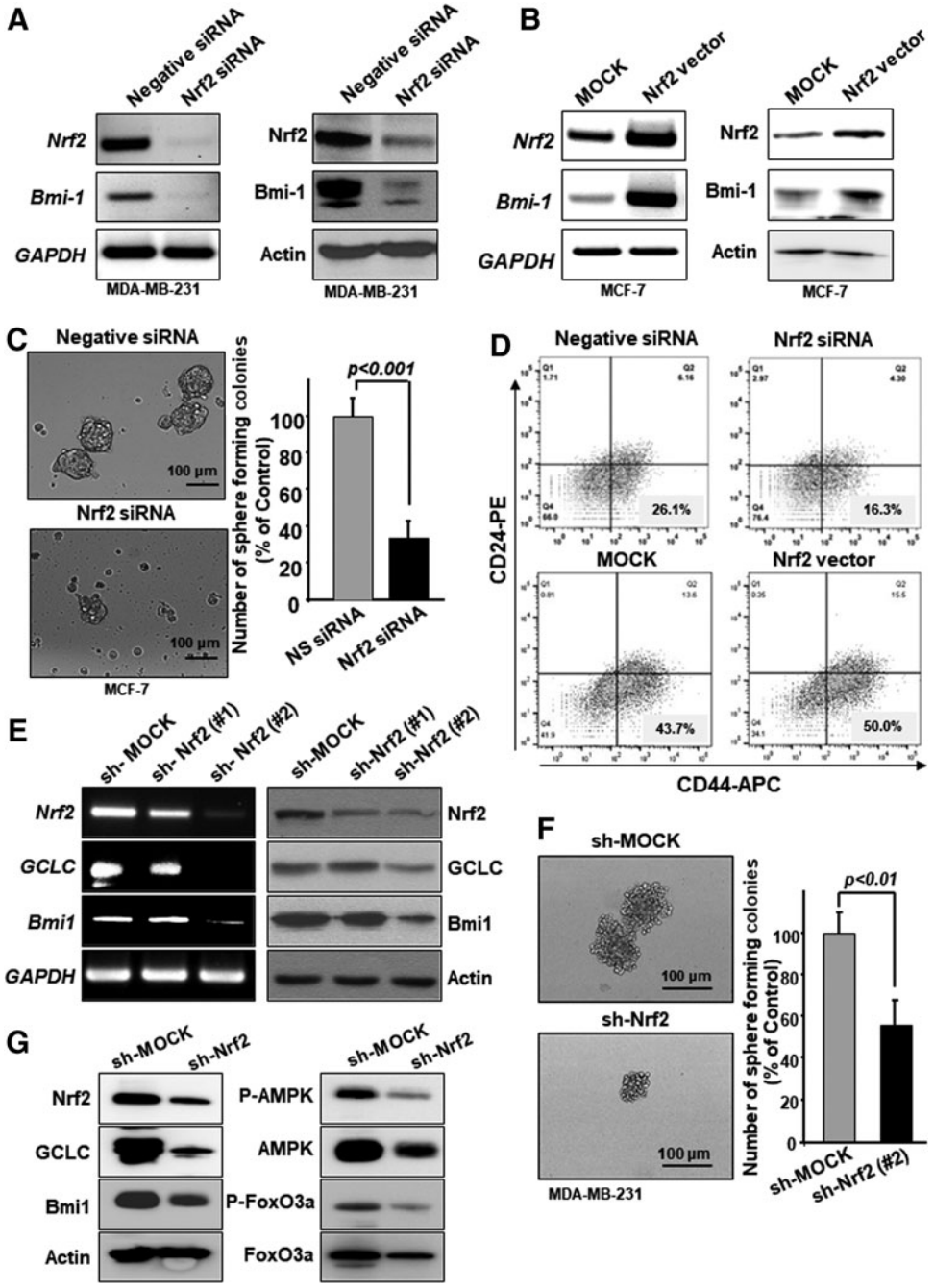

FIG. 6. The effect of Nrf2 on the self-renewal activity of breast cancer cells. **(A)** MDA-MB-231 cells were transfected with Nrf2-siRNA or scrambled siRNA for 72 h, and then the levels of *Bmi-1* mRNA transcript and protein were assessed by RT-PCR and Western blot analysis, respectively. **(B)** MCF-7 cells were transiently transfected with empty (MOCK) or Nrf2 overexpression vector, and *Bmi-1* mRNA and protein expression was determined. **(C)** MCF-7 cells were transfected with scrambled siRNA or Nrf2-specific siRNA for 72 h, followed by sphere-forming culture for additional 5 days. Sphere forming colonies were examined by phase-contrast microscopy (magnification × 100). Pictures are representative photomicrographs of mammospheres, and graph bars are presented as the number of sphere cells ($n = 3$ per treatment group, size >100 μm). Scale bar, 100 μm **(D)** MCF-7 cells were transfected with negative/Nrf2 siRNAs or MOCK/Nrf2 vector for 72 h, followed by staining sphere-forming cells for additional 5 days with anti-CD44-APC and anti-CD24-PE antibodies. Flow cytometric *dot plots* represent changes in the proportion of $CD44^{high}/CD24^{low}$ cells. Quadrant analysis of fluorescence intensity of gated cells in FL2 and FL4 channels was from 10,000 events. **(E)** Endogenous Nrf2 expression was inhibited by two independent Nrf2-targeting shRNA lentiviruses (Nrf2-shRNA #1 or #2) in MDA-MB-231 cells. Efficiency of Nrf2 knockdown and its effect on the expression of GCLC and Bmi1 were assessed by RT-PCR and Western blot analysis. **(F)** Control and Nrf2-shRNA expressing MDA-MB-231 cells were cultured on ultralow adherence plates for 5 days to generate primary mammospheres, and then the primary mammospheres were dissociated and cultured for additional 5 days to generate secondary mammospheres. Sphere forming colonies were examined by phase-contrast microscopy. Scale bar, 100 μm. **(G)** The expression of indicated proteins was analyzed by immunoblot analysis with total cell lysates of control and Nrf2-shRNA MDA-MB-231 mammospheres.

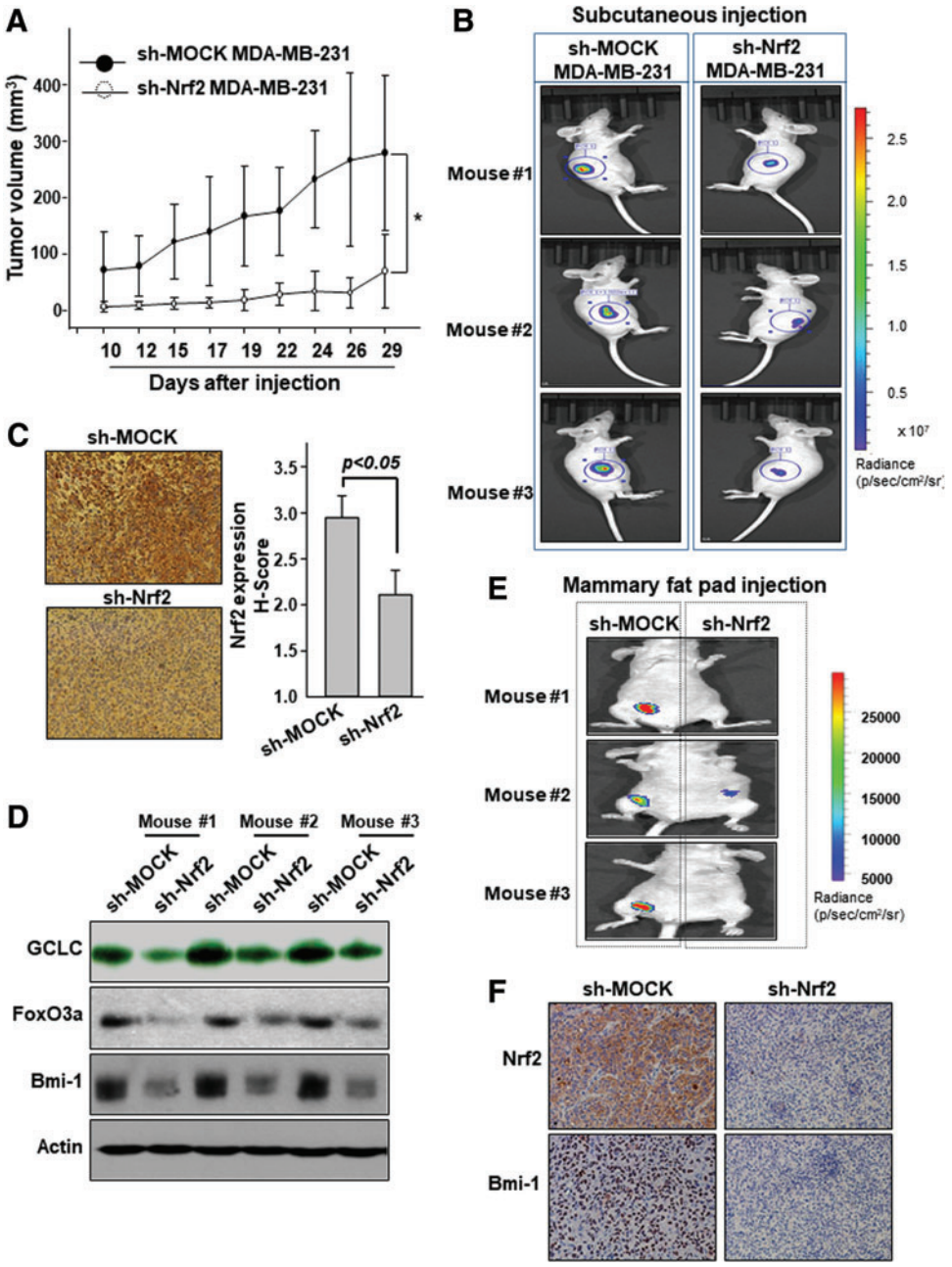

FIG. 7. Knockdown of Nrf2 attenuates the tumorigenicity and self-renewal activity of breast cancer cells *in vivo*. **(A)** The subcutaneous xenograft tumor growth of MDA-MB-231 cells with stable knockdown of Nrf2 was quantified with a manual caliper two to three times per week and compared with that of control GFP-MDA-MB-231 cells. Values are means ± SD. *Significant difference between control and Nrf2 knockdown tumors at $p < 0.05$. **(B)** Established control GFP or Nrf2 knockdown stable MDA-MB-231 cells were injected subcutaneously into the *right* and *left* side flanks of nude mice, respectively ($n = 5$ per group). After 4 weeks, tumor GFP images were captured by the IVIS system. **(C)** Sections from xenograft tissues of mice injected with MDA-MB-231 were immunostained for the Nrf2. **(D)** Whole tissue lysates were separated by sodium dodecyl sulfate-polyacrylamide gel electrophoresis and immunoblotted with GCLC, FoxO3a, and Bmi-1 antibodies. **(E)** One thousand cells from established control GFP or MDA-MB-231 mammospheres stably silenced for Nrf2 expression were injected into their mammary fat pad. After 10 weeks, bioluminescence images of mice bearing primary tumors were taken using an IVIS spectrum. **(F)** Sections from mammary fat pad tissues injected with MDA-MB-231 mammospheres were immunostained for the Nrf2 and Bmi-1. GFP, green fluorescence protein; IVIS, *in vivo* imaging system. Color images are available online.

mammospheres derived from MCF-7 cells were reduced by silencing Nrf2 as well as pharmacological inhibition of its target protein, GCLC. In addition, ROS levels were found to be decreased in the $CD24^{low}/CD44^{high}$ breast cancer stem-like cells compared with parent cancer cells. In accord with these findings, we noticed a substantially elevated level of intracellular GSH in breast cancer stem-like cells.

Mizuno *et al.* have shown that aldehyde dehydrogenase (ALDH)-positive clear carcinoma cells retain a lower level of ROS than cells with low ALDH activity, and that increased

HO-1 and SOD2 expression is regulated by Nrf2 (28). Notably, Nrf2 can be a therapeutic target for chemoresistant breast cancer cells and CSCs (38, 43). Syu *et al.* have reported that overexpression of Nrf2 attenuates the apoptosis induced by cisplatin in human breast cancer (MCF-7) cells under hypoxia, and the drug resistance in Nrf2 overexpressing cells was decreased by chemical inhibition of GCLC or its gene silencing (43).

Recently, Ryoo *et al.* reported that CD44 elevation led to p62-associated Nrf2 activation in doxorubicin-resistant MCF-7 cells (36). Autophagy activation might be an essential cellular process for adaptation and survival of CSCs; however, it is currently not clear how p62 is elevated by autophagic alteration in CSCs (36). It will be important to explore the relevance between autophagy and redox signaling in CSCs. Autophagy can be initiated by increased levels of ROS in various cancer cells, which triggers the activation of Notch1, ALDH, and Nrf2 signaling. The role of autophagy in cancer is still a double-edged sword. Bactericidal antibiotics used in combination with an autophagy blocker decreases tumor growth, whereas the use of an autophagy inhibitor with the anticancer drug leads to increased cell death (1, 34). In addition, many transcription factors including NF-κB, HIF-1α, Nrf2, and Notch are regulated by the cellular redox status. Kipp *et al.* observed that the activation of Nrf2, HIF, and NF-κB was induced throughout the whole spheroids of colon cancer cells (20). Particularly, HIF and Nrf2 are specifically activated in the core of larger spheroids (20).

An intriguing question is how GSH that accumulates in relatively large amounts in sphere-forming cells can modulate the self-renewal activity of breast cancer stem-like cells. The alteration of nuclear redox conditions influences chromatin conformation and stability. Glutathionylation of histone H3 during the translocation of GSH into the nucleus modulates the chromatin availability to replicative or transcriptional machineries by affecting interactions between H3 and nuclear proteins, such as lamin B receptor and heterochromatin protein 1 (25). In addition, GSH functions as an intracellular metal chelator (11). GSH supplementation improved lipid metabolism through increased expression of AMPK in skeletal muscles (3). Moreover, Dong *et al.* have revealed that both oxidative stress and ROS inhibition can activate AMPK through different mechanisms in a diabetic rat model. According to this study, AMPK activation by low ROS is due to redox modification, specifically the *S*-glutathionylation of cysteine residues in its alpha-subunit (10). It has been suggested that FoxO3a phosphorylation by AMPK facilitates the recruitment of the transcriptional complex at the specific target promoter. AMPK activation is associated with an increase in NAD^+ levels, leading to activation of SIRT1 and upregulation of its downstream targets including FoxO3a (7). We speculate that the regulation of FoxO3a by AMPK may play a crucial role in fine-tuning of gene expression programs that control redox balance.

It is widely accepted that FoxO3 is a key regulator of self-renewal activity of stem cells depending on cellular redox status (27). Loss of FoxO3 is associated with an increased ROS level as well as decreased expression of SOD2 and catalase (27). The results from our present study corroborate the possible involvement of FoxO3a in reducing the intracellular ROS levels, thereby conferring acquired self-renewal capacity in breast CSCs. Doxorubicin-resistant breast cancer cells show FoxO3a predominantly expressed in the nucleus, which is then available for the phosphorylation of Akt (14). Notably, the Ser-7 residue of FoxO3a is the only phosphorylation site associated with its nuclear enrichment, thus providing a useful molecular marker of nuclear FoxO3a (14).

FoxO3a is a transcription factor, which binds to a consensus DNA sequence (G/C/A) (T/C/A) AAA (T/C) called forkhead response element. FoxO3a regulates the transcription of a wide variety of genes, such as Bim and Fas ligand involved in regulating cell survival and death (2). In addition, FoxO3a promotes the transcription of pluripotency factor Nanog gene, and then stimulates enrichment of breast CSCs (22). Interestingly, high expression of FoxO3 was associated with poor prognosis in breast cancer patients who received chemotherapy (22).

Dysregulated expression of Bmi-1 has been frequently observed in several types of cancer (19, 40). Consistent with our results, there has been correlation between Nrf2 accumulation and Bmi-1 expression in cervical and gastric CSCs (17, 49). Our study provides an insight into the mechanism underlying upregulation of Bmi-1 expression by Nrf2 in CSCs (Fig. 8). One of the most salient features of our findings is that nuclear FoxO3a can directly bind to the promoter of the gene encoding Bmi-1.

In conclusion, Nrf2-mediated upregulation of GCLC expression and GSH biosynthesis suppress intracellular ROS accumulation. This, in turn, induces the nuclear localization of FoxO3a, which binds to the Bmi-1 promoter, enhancing self-renewal activity and tumorigenic potential of breast CSCs.

Materials and Methods

Reagents

Dulbecco's modified Eagle's medium (DMEM), Rosewell Park Memorial Institute (RPMI) 1640 medium, and Dulbecco's modified Eagle's Medium Nutrient Mixture F-12 (DMEM/F-12) were purchased from Gibco BRL (Grand Island, NY). TRIzol®, MitoSOX™, DHE, and DCF-DA were obtained from Invitrogen (Carlsbad, CA). Primary antibodies for Bmi1, CD44, and Foxo3a were purchased from Cell Signaling Technology (Danvers, MA). Primary antibody against GCLC was obtained from Novus Biologicals (Littleton, CO). Primary antibodies against Nrf2 and β-actin were purchased from Santa Cruz (Santa Cruz, CA). Antibodies against CD24 and CD44 were purchased from BD Biosciences (Bedford, MA). Bicinchoninic acid (BCA) protein assay reagent was a product of Pierce Biotechnology (Rockfold, IL). GSH-MEE, BSO, and H_2O_2 were purchased from Sigma-Aldrich (St. Louis, MO).

Cell culture

Human breast cancer (MCF-7, MDA-MB-231) cell lines were maintained in RPMI 1640 and DMEM medium supplemented with 10% fetal bovine serum (FBS; GenDEPOT, Barker, TX) and 100 ng/mL penicillin/streptomycin/fungizone mixture at 37°C in a humidified atmosphere of 5% CO_2/95% air.

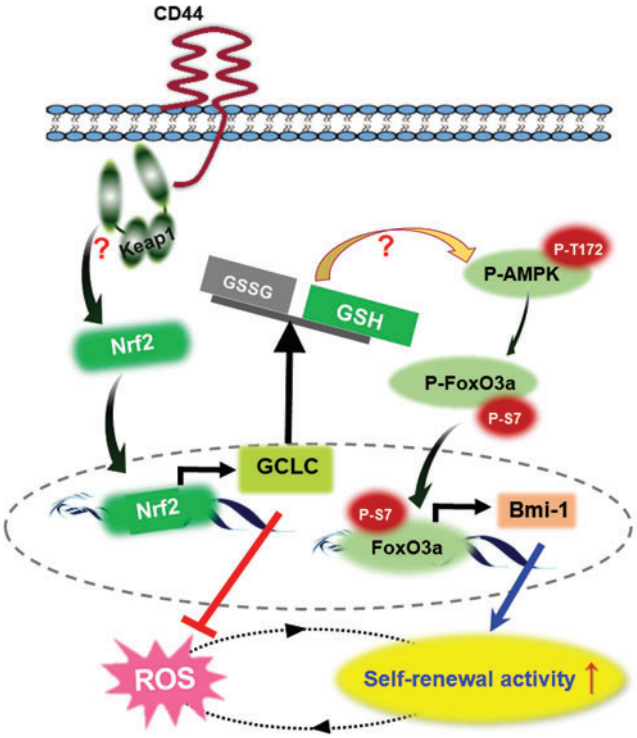

FIG. 8. Schematic diagram illustrating stimulation of self-renewal activity of breast cancer stem-like cells through Nrf2-mediated GCLC upregulation. In breast cancer stem-like cells, expression of CD44 induces nuclear accumulation of Nrf2. Nrf2 upregulates GCLC expression by binding to its promoter, and consequent overproduction of GSH suppresses ROS accumulation. This, in turn, induces the activation of AMPK and FoxO3a through phosphorylation. FoxO3a binds to the Bmi-1 promoter. In response to Nrf2 overactivation, genes regulating the redox status are upregulated, which contributes to the self-renewal activity and tumorigenesis. Color images are available online.

Mammosphere formation assay

MCF-7 (5×10^3 cells per well) and MDA-MB-231 (1×10^4 cells per well) cells were cultured in a serum-free DMEM/F12 medium supplemented with B27 (GIBCO), 20 ng/mL epidermal growth factor (Sigma-Aldrich), 20 ng/mL basic fibroblast growth factor (Peprotech, Rocky Hill, NJ), and 4 ng/mL heparin (Sigma-Aldrich) in six-well ultralow attachment surface plates (Corning, NY). After 5 days, primary mammospheres formation was examined using an inverted microscope. To culture secondary mammospheres, primary mammospheres were gently collected and dissociated into a single-cell suspension using 40-μm strainer. Single cells were counted and then seeded again for another 5 days with addition of 1 mL medium every 2–3 days. After 5 days, secondary mammospheres formation was examined using an inverted microscope, and the number of mammospheres formed (>100 μm) was quantified.

Flow cytometric analysis

MCF-7 cells were collected and washed with phosphate-buffered saline (PBS), and dissociated with Accutase solution (Sigma-Aldrich). Cells were then counted and washed with PBS containing 2% FBS and 0.1% Tween-20. Cells were stained with CD24-propidium iodide and CD44-APC from BD Biosciences for 30 min at 4°C. Cells were dissociated into single cells by using 40-μm strainer, and then the population of $CD44^+/CD24^-$ cells was measured using BD FACSCalibur (Becton Dickinson Biosciences, San Jose). To isolate CSC and non-CSC populations from breast cancer cells, cells were stained with the above antibodies, and the cells were sorted using BD FACSAria™ III cell sorter (Becton Dickinson Biosciences).

Determination of intracellular glutathione levels

Intracellular glutathione levels were determined using the bioluminescent Promega GSH/GSSG-Glo™ assay kit (Promega, Mannheim, Germany) according to manufacturer's protocols. Luminescence was detected using SpectraMax i3 Multi-Mode Microplate Reader (Molecular Devices, Sunnyvale, CA).

Analysis of intracellular ROS accumulation

Intracellular accumulation of ROS was assessed by using redox-sensitive dye DCF-DA. Cells were washed once with Hanks' balanced salt solution and loaded with 10 μM DCF-DA for 30 min at 37°C to assess ROS-mediated oxidation of the fluorescent compound DCF. Fluorescence of oxidized DCF was analyzed by flow cytometry.

Western blot analysis

Breast cancer cells were lysed in radioimmunoprecipitation assay lysis buffer (150 mM NaCl, 0.5% Triton × 100, 50 mM Tri-HCl (pH 7.4), 25 mM NaF, 20 mM EGTA, 1 mM dithiothreitol, 1 mM Na_3VO_4, 0.1 mM PMSF, protease inhibitor cocktail tablets) for 15 min on ice followed by centrifugation at 13,000 g for 20 min. The protein concentration of the supernatant was measured by using BCA reagents (Thermo-Scientific, Rockford, IL). Protein (30 μg) was separated by running through 8%–12% sodium dodecyl sulfate-polyacrylamide gel electrophoresis gel and transferred to the polyvinylidene fluoride membrane (Gelman Laboratory, Ann Arbor, MI). The blots were blocked with 5% nonfat dry milk/Tris-buffered saline buffer containing 0.1% Tween-20 (TBST) for 1 h at room temperature. The membranes were incubated overnight at 4°C with indicated primary antibodies. The blots were rinsed three times with TBST buffer for 10 min each. Washed blots were incubated with 1:5000 dilutions of horseradish peroxidase-conjugated secondary antibody (Thermoscientific) for 1 h and washed again three times with TBST buffer. The transferred proteins were visualized with an enhanced chemiluminescence detection kit (Amersham Pharmacia Biotech, Buckinghamshire, United Kingdom).

Preparation of cytosolic and nuclear proteins

Cells were gently washed twice with ice-cold PBS, scraped in 1 mL PBS and centrifuged at 12,000 g for 30 s at 4°C. Pellets were suspended in 200 μL of hypotonic buffer A (10 mM HEPES, pH 7.9; 10 mM KCl; 2 mM $MgCl_2$; 1 mM DTT; 0.1 mM EDTA; 0.1 mM PMSF) for 15 min on ice, and 12.5 μL of 10% Nondiet P-40 solution was added for 5 min. The mixture was then centrifuged for 6 min at 12,000 g,

washed once with 400 μL of PBS, and suspended in 70 μL of buffer C (50 m*M* HEPES, pH 7.9; 50 m*M* KCl; 300 m*M* NaCl; 0.1 m*M* EDTA; 1 m*M* DTT; 0.1 m*M* PMSF; and 10% glycerol) for 20 min on ice and centrifuged for 6 min at 14,000 *g*. The supernatant containing nuclear proteins was collected and stored at −70°C after determination of the protein concentration.

Immunofluorescence microscopy

To determine the localization of indicated proteins, we adopted the immunocytochemical method that utilized a monoclonal antibody recognizing Nrf2 and FoxO3a. Cells (1×10^5 cells/600 μL in four-well chamber slides) were fixed in 95% methanol/5% acetic acid solution for 10 min at −20°C. After a rinse with PBS, cells were blocked for 1h at room temperature in fresh blocking buffer (0.5% Tween 20 in PBS, pH 7.4, containing 10% normal goat serum). Dilutions (1:100) of primary antibodies were made in PBS with 1% bovine serum albumin, and cells were incubated overnight at 4°C. After three washes with PBS containing 0.1% Tween 20 (PBST), the cells were incubated with FITC-conjugated secondary antibody in PBST with 3% bovine serum albumin for 1h at room temperature. Cells were rinsed with PBS, and stained cells were analyzed under a fluorescence microscope and photographed.

Reverse transcription-polymerase chain reaction

Total RNA was isolated from each cell by using TRIzol reagent (Invitrogen) according to the manufacturer's protocol. One microgram of total RNA was reverse transcribed with murine leukemia virus reverse transcriptase (Promega, Madison, WI). Polymerase chain reaction (PCR) was carried out in a thermos-cycler using specific primers for *Nrf2*, *GCLC*, *Bmi-1,* and *GAPDH*. The primers employed were (forward and reverse, respectively): *Nrf2*, 5′-ACTGGTT GGGGTCTTCTGTG-3′ and 5′-CGGTATGCAACAGGAC ATTG-3′, 263 bp; *GCLC*, 5′-TGAAGGGACACCAGG ACAGCC-3′ and 5′-GCAGTGTGAACCCAGGACAGC-3′, 167 bp; *Bmi-1*, 5′-CCAGGGCTTTTCAAAAATGA-3′ and 5′-GCATCACAGTCATTGCTGCT-3′, 271 bp; *GAPDH*, 5′-GCATGGCCTTCCGTGTCCCC-3′ and 5′-CAATGCCA GCCCCAGCGTCA-3′, 216 bp. Amplification products were resolved by 1.5%–2% agarose gel electrophoresis, stained with ethidium bromide and photographed under ultraviolet light.

Transient transfection of siRNA and plasmid

MCF-7 and MDA-MB-231 cells were plated at a confluence of 60% in 60-mm dish and grown in complete growth media. Nrf2, CD44 and FoxO3a siRNA (25 n*M*) and Nrf2 plasmid were transfected into MCF-7 cells with lipofectamine RNAiMAX or lipofectamine 2000 (Invitrogen) reagents. The siRNA sequences were (forward and reverse, respectively) as follows: *Nrf2*, 5′-AAGAGUAUGAGUGG AAAAACTT-3′ and 5′-GUUUUUCCAGCUCAUACUC UUTT-3′; *CD44*, 5′-UAUUCCACGUGGAGAAAATT-3′ and 5′-UUUUUCUCCACGUGGAAUACA-3′; *FoxO3a*, 5′-CAGUUCUAACUUCACUGUU-3′ and 5′-AACAGU GAAGUUAGAACUG-3′. Plasmid of pcDNA3.1-EGFP-C4-human Nrf2 was obtained from Adggene (plasmid #21549).

ChIP assay

After formaldehyde crosslinking, cells were harvested, and the ChIP assay was performed using EZ ChIP kit according to the manufacturer's protocol (Millipore). Chromatin was immunoprecipitated with antibody against the FoxO3a or IgG as a negative control. Input and bound DNA were purified using the Genomic DNA Extraction Kit (SolGent, Daejeon, Korea). PCR was performed against FoxO3a binding region of the Bmi-1 promoter. The primer sequences were 5′-TTGTTTGGATCTGAGTTCGTGTG3′ (forward) and 5′-ATCGCATCGTTTCCTCCGTG-3′. Reaction conditions were as follows: initial denaturation (5 min at 94°C) was followed by 40 cycles for 1 min at 94°C, 1 min at 55°C, and 1 min at 72°C. PCR was completed by 10 min at 72°C, and products were separated on 2.5% agarose gel.

Knockdown of Nrf2 in breast cancer cells

A set of two human (SH-003755) specific SMART vector 2.0 lentiviral shRNA particles (10^8 TU/mL) for NFE2L2 were purchased from Thermo Fisher Scientific Dharmacon (Lafayette, CO). The vector had an human cytomegalovirus promoter, a TurboGFP reporter gene, and a puromycin selection gene. SMART vector 2.0 nontargeting shRNA control particles (10^8 TU/mL) were designed as a negative control. MDA-MB-231 cells were cultured in DMEM with 10% FBS in the presence of antibiotics, and viral particles (NFE2L2 and nontargeting control) were added with a multiplicity of infection of 3.0 for cells. TurboGFP-expression was analyzed using microscopy and GFP-positive cells selected using puromycin (5 μg/mL). The selected cells were maintained in culture media containing puromycin at 0.5 μg/mL until further use. Nrf2 silencing was verified by Western blot and mRNA quantification.

Mouse studies

Animal experiments were conducted in accordance with Guide for the Care and Use of Laboratory Animals, and approved by the Institutional Animal Care and Use Committee of Seoul National University (SNU protocol #160622-10). For a xenograft tumor model, MDA-MB-231 (2×10^6 cells per mouse in 50 μL containing Matrigel) was injected into 6-week-old female BALB/c nu/nu mice. After 10 days, tumor volume was determined by measuring the diameters of tumors with a caliper every 2 or 3 days. Tumor volumes were calculated according to the following formula: (length)×(width)×(height)×0.52. For an orthotopic tumor model using mammosphere cells, MDA-MB-231 mammosphere cells (1×10^5 cells per mouse in 50 μL containing Matrigel) were injected into 6-week-old female nude mice at mammary fat pad. Bioluminescence imaging was obtained by the IVIS spectrum micro CT and Living Image (ver. 4.2) software (PerkinElmer).

Public data resources

The clinical data of breast cancer were obtained from both TCGA and GSE2034. The Cancer Genome Atlas (TCGA) clinical data for breast cancer patients ($n=1108$) were retrieved from cBioPortal, including RNA-seq gene expression profiles. Dataset for recurrent breast cancer patients was

obtained from Gene Expression Omnibus. Gene expression profiles of breast cancer from GSE2034 (nonrelapse [$n = 179$] and relapse [$n = 107$]) and GSE1456 (nonrelapse [$n = 119$] and relapse [$n = 40$]) were used for analysis.

Statistical analysis

When necessary, data were represented as means±SD of at least three independent experiments, and statistical analysis between groups was performed using Student's *t*-test.

Author Disclosure Statement

No competing financial interests exist.

Funding Information

This study was supported by the Global Core Research Center (GCRC) grant (No. 2011-0030001) and Basic Science Research Program grant (No. 2013R1A1A2012429 and 2016R1A6A3A11935082) from the National Research Foundation (NRF) of Republic of Korea.

Supplementary Material

Supplementary Figure S1
Supplementary Figure S2
Supplementary Figure S3
Supplementary Figure S4
Supplementary Figure S5
Supplementary Figure S6
Supplementary Figure S7
Supplementary Figure S8
Supplementary Figure S9
Supplementary Figure S10
Supplementary Figure S11
Supplementary Figure S12
Supplementary Figure S13

References

1. Abad E, Garcia-Mayea Y, Mir C, Sebastian D, Zorzano A, Potesil D, Zdrahal Z, Lyakhovich A, and Lleonart ME. Common metabolic pathways implicated in resistance to chemotherapy point to a key mitochondrial role in breast cancer. *Mol Cell Proteomics* 18: 231–244, 2019.
2. Accili D and Arden KC. FoxOs at the crossroads of cellular metabolism, differentiation, and transformation. *Cell* 117: 421–426, 2004.
3. Aoi W, Ogaya Y, Takami M, Konishi T, Sauchi Y, Park EY, Wada S, Sato K, and Higashi A. Glutathione supplementation suppresses muscle fatigue induced by prolonged exercise via improved aerobic metabolism. *J Int Soc Sports Nutr* 12: 7, 2015.
4. Aquilano K, Baldelli S, and Ciriolo MR. Glutathione: new roles in redox signaling for an old antioxidant. *Front Pharmacol* 5: 196, 2014.
5. Chen C, Liu Y, Liu Y, and Zheng P. The axis of mTOR-mitochondria-ROS and stemness of the hematopoietic stem cells. *Cell Cycle* 8: 1158–1160, 2009.
6. Cheng X and O'Neill HC. Oncogenesis and cancer stem cells: current opinions and future directions. *J Cell Mol Med* 13: 4377–4384, 2009.
7. Chiacchiera F and Simone C. The AMPK-FoxO3A axis as a target for cancer treatment. *Cell Cycle* 9: 1091–1096, 2010.
8. Dean M, Fojo T, and Bates S. Tumour stem cells and drug resistance. *Nat Rev Cancer* 5: 275–284, 2005.
9. Diehn M, Cho RW, Lobo NA, Kalisky T, Dorie MJ, Kulp AN, Qian D, Lam JS, Ailles LE, Wong M, Joshua B, Kaplan MJ, Wapnir I, Dirbas FM, Somlo G, Garberoglio C, Paz B, Shen J, Lau SK, Quake SR, Brown JM, Weissman IL, and Clarke MF. Association of reactive oxygen species levels and radioresistance in cancer stem cells. *Nature* 458: 780–783, 2009.
10. Dong K, Wu M, Liu X, Huang Y, Zhang D, Wang Y, Yan LJ, and Shi D. Glutaredoxins concomitant with optimal ROS activate AMPK through *S*-glutathionylation to improve glucose metabolism in type 2 diabetes. *Free Radic Biol Med* 101: 334–347, 2016.
11. Freedman JH, Ciriolo MR, and Peisach J. The role of glutathione in copper metabolism and toxicity. *J Biol Chem* 264: 5598–5605, 1989.
12. Garcia-Gimenez JL, Markovic J, Dasi F, Queval G, Schnaubelt D, Foyer CH, and Pallardo FV. Nuclear glutathione. *Biochim Biophys Acta* 1830: 3304–3316, 2013.
13. Gorrini C, Harris IS, and Mak TW. Modulation of oxidative stress as an anticancer strategy. *Nat Rev Drug Discov* 12: 931–947, 2013.
14. Ho KK, McGuire VA, Koo CY, Muir KW, de Olano N, Maifoshie E, Kelly DJ, McGovern UB, Monteiro LJ, Gomes AR, Nebreda AR, Campbell DG, Arthur JS, and Lam EW. Phosphorylation of FOXO3a on Ser-7 by p38 promotes its nuclear localization in response to doxorubicin. *J Biol Chem* 287: 1545–1555, 2012.
15. Hu J, Li G, Zhang P, Zhuang X, and Hu G. A CD44v(+) subpopulation of breast cancer stem-like cells with enhanced lung metastasis capacity. *Cell Death Dis* 8: e2679, 2017.
16. Jang YY and Sharkis SJ. A low level of reactive oxygen species selects for primitive hematopoietic stem cells that may reside in the low-oxygenic niche. *Blood* 110: 3056–3063, 2007.
17. Jia Y, Chen J, Zhu H, Jia ZH, and Cui MH. Aberrantly elevated redox sensing factor Nrf2 promotes cancer stem cell survival via enhanced transcriptional regulation of ABCG2 and Bcl-2/Bmi-1 genes. *Oncol Rep* 34: 2296–2304, 2015.
18. Kakehashi A, Ishii N, Sugihara E, Gi M, Saya H, and Wanibuchi H. CD44 variant 9 is a potential biomarker of tumor initiating cells predicting survival outcome in hepatitis C virus-positive patients with resected hepatocellular carcinoma. *Cancer Sci* 107: 609–618, 2016.
19. Kim JH, Yoon SY, Kim CN, Joo JH, Moon SK, Choe IS, Choe YK, and Kim JW. The Bmi-1 oncoprotein is overexpressed in human colorectal cancer and correlates with the reduced p16INK4a/p14ARF proteins. *Cancer Lett* 203: 217–224, 2004.
20. Kipp AP, Deubel S, Arner ESJ, and Johansson K. Time- and cell-resolved dynamics of redox-sensitive Nrf2, HIF and NF-κB activities in 3D spheroids enriched for cancer stem cells. *Redox Biol* 12: 403–409, 2017.
21. Klotz LO, Sanchez-Ramos C, Prieto-Arroyo I, Urbanek P, Steinbrenner H, and Monsalve M. Redox regulation of FoxO transcription factors. *Redox Biol* 6: 51–72, 2015.
22. Lu H, Samanta D, Xiang L, Zhang H, Hu H, Chen I, Bullen JW, and Semenza GL. Chemotherapy triggers HIF-1-

dependent glutathione synthesis and copper chelation that induces the breast cancer stem cell phenotype. *Proc Natl Acad Sci U S A* 112: E4600–E4609, 2015.
23. Lukacs RU, Memarzadeh S, Wu H, and Witte ON. Bmi-1 is a crucial regulator of prostate stem cell self-renewal and malignant transformation. *Cell Stem Cell* 7: 682–693, 2010.
24. Markovic J, Borras C, Ortega A, Sastre J, Vina J, and Pallardo FV. Glutathione is recruited into the nucleus in early phases of cell proliferation. *J Biol Chem* 282: 20416–20424, 2007.
25. Markovic J, Garcia-Gimenez JL, Gimeno A, Vina J, and Pallardo FV. Role of glutathione in cell nucleus. *Free Radic Res* 44: 721–733, 2010.
26. McMahon M, Itoh K, Yamamoto M, Chanas SA, Henderson CJ, McLellan LI, Wolf CR, Cavin C, and Hayes JD. The Cap'n'Collar basic leucine zipper transcription factor Nrf2 (NF-E2 p45-related factor 2) controls both constitutive and inducible expression of intestinal detoxification and glutathione biosynthetic enzymes. *Cancer Res* 61: 3299–3307, 2001.
27. Miyamoto K, Araki KY, Naka K, Arai F, Takubo K, Yamazaki S, Matsuoka S, Miyamoto T, Ito K, Ohmura M, Chen C, Hosokawa K, Nakauchi H, Nakayama K, Nakayama KI, Harada M, Motoyama N, Suda T, and Hirao A. Foxo3a is essential for maintenance of the hematopoietic stem cell pool. *Cell Stem Cell* 1: 101–112, 2007.
28. Mizuno T, Suzuki N, Makino H, Furui T, Morii E, Aoki H, Kunisada T, Yano M, Kuji S, Hirashima Y, Arakawa A, Nishio S, Ushijima K, Ito K, Itani Y, and Morishige K. Cancer stem-like cells of ovarian clear cell carcinoma are enriched in the ALDH-high population associated with an accelerated scavenging system in reactive oxygen species. *Gynecol Oncol* 137: 299–305, 2015.
29. Nguyen T, Nioi P, and Pickett CB. The Nrf2-antioxidant response element signaling pathway and its activation by oxidative stress. *J Biol Chem* 284: 13291–13295, 2009.
30. Ogasawara MA and Zhang H. Redox regulation and its emerging roles in stem cells and stem-like cancer cells. *Antioxid Redox Signal* 11: 1107–1122, 2009.
31. Paranjape AN, Balaji SA, Mandal T, Krushik EV, Nagaraj P, Mukherjee G, and Rangarajan A. Bmi1 regulates self-renewal and epithelial to mesenchymal transition in breast cancer cells through Nanog. *BMC Cancer* 14: 785, 2014.
32. Paul MK, Bisht B, Darmawan DO, Chiou R, Ha VL, Wallace WD, Chon AT, Hegab AE, Grogan T, Elashoff DA, Alva-Ornelas JA, and Gomperts BN. Dynamic changes in intracellular ROS levels regulate airway basal stem cell homeostasis through Nrf2-dependent Notch signaling. *Cell Stem Cell* 15: 199–214, 2014.
33. Pearson T, Kabayo T, Ng R, Chamberlain J, McArdle A, and Jackson MJ. Skeletal muscle contractions induce acute changes in cytosolic superoxide, but slower responses in mitochondrial superoxide and cellular hydrogen peroxide. *PLoS One* 9: e96378, 2014.
34. Poillet-Perez L, Despouy G, Delage-Mourroux R, and Boyer-Guittaut M. Interplay between ROS and autophagy in cancer cells, from tumor initiation to cancer therapy. *Redox Biol* 4: 184–192, 2015.
35. Proctor E, Waghray M, Lee CJ, Heidt DG, Yalamanchili M, Li C, Bednar F, and Simeone DM. Bmi1 enhances tumorigenicity and cancer stem cell function in pancreatic adenocarcinoma. *PLoS One* 8: e55820, 2013.
36. Ryoo IG, Choi BH, Ku SK, and Kwak MK. High CD44 expression mediates p62-associated NFE2L2/NRF2 activation in breast cancer stem cell-like cells: implications for cancer stem cell resistance. *Redox Biol* 17: 246–258, 2018.
37. Ryoo IG, Choi BH, and Kwak MK. Activation of NRF2 by p62 and proteasome reduction in sphere-forming breast carcinoma cells. *Oncotarget* 6: 8167–8184, 2015.
38. Ryoo IG, Kim G, Choi BH, Lee SH, and Kwak MK. Involvement of NRF2 signaling in doxorubicin resistance of cancer stem cell-enriched colonospheres. *Biomol Ther* 24: 482–488, 2016.
39. Shi X, Zhang Y, Zheng J, and Pan J. Reactive oxygen species in cancer stem cells. *Antioxid Redox Signal* 16: 1215–1228, 2012.
40. Silva J, Garcia V, Garcia JM, Pena C, Dominguez G, Diaz R, Lorenzo Y, Hurtado A, Sanchez A, and Bonilla F. Circulating Bmi-1 mRNA as a possible prognostic factor for advanced breast cancer patients. *Breast Cancer Res* 9: R55, 2007.
41. Singh A and Settleman J. EMT, cancer stem cells and drug resistance: an emerging axis of evil in the war on cancer. *Oncogene* 29: 4741–4751, 2010.
42. Skvortsova I, Debbage P, Kumar V, and Skvortsov S. Radiation resistance: cancer stem cells (CSCs) and their enigmatic pro-survival signaling. *Semin Cancer Biol* 35: 39–44, 2015.
43. Syu JP, Chi JT, and Kung HN. Nrf2 is the key to chemotherapy resistance in MCF7 breast cancer cells under hypoxia. *Oncotarget* 7: 14659–14672, 2016.
44. Taguchi K, Motohashi H, and Yamamoto M. Molecular mechanisms of the Keap1-Nrf2 pathway in stress response and cancer evolution. *Genes Cells* 16: 123–140, 2011.
45. Tothova Z, Kollipara R, Huntly BJ, Lee BH, Castrillon DH, Cullen DE, McDowell EP, Lazo-Kallanian S, Williams IR, Sears C, Armstrong SA, Passegue E, DePinho RA, and Gilliland DG. FoxOs are critical mediators of hematopoietic stem cell resistance to physiologic oxidative stress. *Cell* 128: 325–339, 2007.
46. Yang B, Ma YF, and Liu Y. Elevated expression of Nrf-2 and ABCG2 involved in multi-drug resistance of lung cancer SP cells. *Drug Res (Stuttg)* 65: 526–531, 2015.
47. Zhang C, Wang HJ, Bao QC, Wang L, Guo TK, Chen WL, Xu LL, Zhou HS, Bian JL, Yang YR, Sun HP, Xu XL, and You QD. NRF2 promotes breast cancer cell proliferation and metastasis by increasing RhoA/ROCK pathway signal transduction. *Oncotarget* 7: 73593–73606, 2016.
48. Zhao Y, Hu X, Liu Y, Dong S, Wen Z, He W, Zhang S, Huang Q, and Shi M. ROS signaling under metabolic stress: cross-talk between AMPK and AKT pathway. *Mol Cancer* 16: 79, 2017.
49. Zhu J, Wang H, Sun Q, Ji X, Zhu L, Cong Z, Zhou Y, Liu H, and Zhou M. Nrf2 is required to maintain the self-renewal of glioma stem cells. *BMC Cancer* 13: 380, 2013.

Address correspondence to:
Prof. Young-Joon Surh
College of Pharmacy
Seoul National University
1 Gwanak-ro
Gwank-gu
Seoul 08826
South Korea

E-mail: surh@snu.ac.kr

Date of first submission to ARS Central, January 27, 2019; date of final revised submission, October 14, 2019; date of acceptance, October 22, 2019.

Abbreviations Used

ALDH = aldehyde dehydrogenase
AMPK = AMP-activated protein kinase
BCA = bicinchoninic acid
BSO = buthionine sulfoximine
ChIP = chromatin immunoprecipitation
CSCs = cancer stem cells
CT = computed tomography
DCF-DA = 2′,7′-dichlorofluorescein diacetate
DHE = dihydroethidium
DMEM = Dulbecco's modified Eagle's medium
FACS = fluorescence-activated cell sorting
FBS = fetal bovine serum
FoxO = Forkhead box O
GCLC = glutamate cysteine ligase catalytic subunit
GFP = green fluorescence protein
GSEA = gene set enrichment analysis
GSH = reduced glutathione
GSH-MEE = glutathione-reduced ethyl ester
GSSG = oxidized glutathione
H_2O_2 = hydrogen peroxide
IHC = immunohistochemical
IVIS = *in vivo* imaging system
Nrf2 = nuclear factor erythroid-derived 2-like 2
P-AMPK = phospho-AMPK
PI = propidium iodide
ROS = reactive oxygen species
RPMI = Rosewell Park Memorial Institute
RT-PCR = reverse transcription-polymerase chain reaction
PBS = phosphate-buffered saline
PBST = PBS containing 0.1% Tween 20
PCR = polymerase chain reaction
shRNA = short hairpin RNA
siRNA = short interfering RNA
TBST = Tris-buffered saline buffer containing 0.1% Tween-20
TCGA = The Cancer Genome Atlas